IOP Publishing Phys. Med. Biol. 65 (2020) 025012 (10pp) https://doi.org/10.1088/1361-6560/ab6241

Physics in Medicine & Biology

IPEM Institute of Physics and Engineering in Medicine

RECEIVED
11 September 2019

REVISED
11 December 2019

ACCEPTED FOR PUBLICATION
16 December 2019

PUBLISHED
16 January 2020

PAPER

Dosimetric impact of soft-tissue based intrafraction motion from 3D cine-MR in prostate SBRT

D M de Muinck Keizer[1,2], C Kontaxis[2], L G W Kerkmeijer, J R N van der Voort van Zyp, C A T van den Berg, B W Raaymakers, J J W Lagendijk and J C J de Boer

University Medical Center Utrecht, Department of Radiotherapy, 3508 GA, Utrecht, The Netherlands

[1] Author to whom any correspondence should be addressed

[2] Joint first author.

E-mail: D.M.deMuinckKeizer@umcutrecht.nl (D M de Muinck Keizer), C.Kontaxis@umcutrecht.nl (C Kontaxis), L.Kerkmeijer@umcutrecht.nl (L G W Kerkmeijer), J.R.N.vanderVoortvanZyp@umcutrecht.nl (J R N van derVoort van Zyp), C.A.T.vandenBerg@umcutrecht.nl (C.A.T. van den Berg), B.W.Raaymakers@umcutrecht.nl (B W Raaymakers), J.J.W.Lagendijk@umcutrecht.nl (J J W Lagendijk) and J.C.J.deBoer-6@umcutrecht.nl (J C J de Boer)

Keywords: dosimetric impact, prostate cancer, intrafraction motion, hypofractionation, soft-tissue registration, tracking, cine-MR

Supplementary material for this article is available online

Abstract

To investigate the dosimetric impact of intrafraction translation and rotation motion of the prostate, as extracted from daily acquired post-treatment 3D cine-MR based on soft-tissue contrast, in extremely hypofractionated (SBRT) prostate patients. Accurate dose reconstruction is performed by using a prostate intrafraction motion trace which is obtained with a soft-tissue based rigid registration method on 3D cine-MR dynamics with a temporal resolution of 11 s. The recorded motion of each time-point was applied to the planning CT, resulting in the respective dynamic volume used for dose calculation. For each treatment fraction, the treatment delivery record was generated by proportionally splitting the plan into 11 s intervals based on the delivered monitor units. For each fraction the doses of all partial plan/dynamic volume combinations were calculated and were summed to lead to the motion-affected fraction dose. Finally, for each patient the five fraction doses were summed, yielding the total treatment dose. Both daily and total doses were compared to the original reference dose of the respective patient to assess the impact of the intrafraction motion. Depending on the underlying motion of the prostate, different types of motion-affected dose distributions were observed. The planning target volumes (PTVs) ensured CTV_30 (seminal vesicles) D99% coverage for all patients, CTV_35 (prostate corpus) coverage for 97% of the patients and GTV_50 (local boost) for 83% of the patients when compared against the strict planning target D99% value. The dosimetric impact due to prostate intrafraction motion in extremely hypofractionated treatments was determined. The presented study is an essential step towards establishing the actual delivered dose to the patient during radiotherapy fractions.

1. Introduction

Hypofractionated or stereotactic body radiotherapy (SBRT) treatments of prostate cancer have gained increased acceptation over the recent years (Loblaw *et al* 2013, Alayed *et al* 2018, Morgan *et al* 2018). This development has been fuelled by the relatively low α/β ratio of prostate tumors (Dasu and Toma-Dasu 2012, van de Water *et al* 2014). Hypofractionated treatments have been associated with good biochemical disease free survival and low toxicity (Widmark *et al* 2016). In addition, hypofractionated radiotherapy has shown to be non-inferior to conventional radiotherapy for intermediate-to-high risk prostate cancer with respect to failure-free survival (Widmark *et al* 2019). Another benefit of hypofractionation is the reduced number of fractions and thus hospital visits for the patients as well as associated costs (Pathmanathan *et al* 2018). Stereotactic hypofractionated treatments require a high degree of accuracy in dose delivery. While delivering a hypofractionated treatment

with an integrated boost to the intraprostatic dominant lesions seems feasible, the applicability of small margins requires monitoring of, and possibly correction for, intrafraction motion (Tree *et al* 2013).

Movement of the prostate during radiotherapy is commonly observed and can range up to 1 cm during a time period of 10 min (Mah *et al* 2002, Li *et al* 2008). This intrafraction motion consists of both drifts and sudden transient motions and occurs mainly in the anterior–posterior and superior–inferior direction (Langen *et al* 2008). Significant intrafraction prostate rotation has been observed about the left–right axis (Huang *et al* 2015).

The impact of intrafraction motion on the accumulated dose has previously been investigated by several different studies (Litzenberg *et al* 2007, Li *et al* 2008, Adamson *et al* 2011, Azcona *et al* 2014, De Leon *et al* 2019). These studies obtained the prostate intrafraction motion based on acquiring fiducial positions with 2D electronic portal imaging device (EPID) images (Azcona *et al* 2014), tracking implanted radiobeacons (Litzenberg *et al* 2007, Li *et al* 2008), by using kV fluoroscopy and posttreatment cone beam computed tomography (CBCT) (Adamson *et al* 2011) or by tracking points of interest on interleaved cine-MR images (De Leon *et al* 2019). To achieve highly accurate dose reconstructions, information on the involved 3D pelvic anatomy should be available during the dose delivery time frame (Poulsen *et al* 2012). The previously mentioned studies did not have this information available and therefore cannot fully describe the dosimetric impact of intrafraction motion.

With the introduction of systems capable of magnetic resonance (MR) guided radiotherapy (Lagendijk *et al* 2014, Mutic and Dempsey 2014, Keall *et al* 2014), new opportunities become available. Due to the fact that these systems can simultaneously acquire MR-images during delivery of radiotherapy, information on the patient's anatomy during beam delivery has become available at a high temporal and spatial resolution (Pathmanathan *et al* 2018). This information can be used to enable the tracking of tumor motion during beam-on and to obtain volumetric soft tissue information of surrounding tissues for accurate dose reconstruction (van Herk *et al* 2018).

During dose reconstruction anatomical motion traces are combined with the treatment delivery record. The anatomical trace may describe translations and rotations but could be extended to include the deformations of the anatomy over time. The treatment delivery record describes the machine parameters of the linear accelerator (linac) during delivery. By combining the two, the appropriate part of the treatment can be delivered on a specific dynamic anatomy and then accumulated on a reference anatomical grid yielding a motion-affected dose distribution.

In principle, this information can be fed back into a dosimetric optimization loop to compensate for interfraction motion in a fraction-by-fraction basis as well as intrafraction motion during delivery. We have previously presented an inter-beam replanning pipeline based on accurate dose reconstruction of the previously delivered dose during treatment using our in-house developed Adaptive Sequencer (ASEQ). Such techniques can ensure target coverage and organ at risk (OAR) sparing and enable safe margin reduction (Kontaxis *et al* 2017b).

The purpose of this study is to investigate the effect of intrafraction motion on the dose distributions of hypofractionated (SBRT) prostate patients using clinically delivered plans. Soft-tissue tracking was used to extract the intrafraction motion of the prostate from full 3D cine-MR data, acquired daily after each radiotherapy fraction of these patients. The magnitude and frequency of prostate intrafraction motion based on these 3D cine-MR images was previously investigated (de Muinck Keizer *et al* 2019a). For each treatment fraction accurate retrospective dose reconstruction is performed by simulating the intrafraction motion using the respective daily motion trace.

2. Material and methods

Twenty-nine prostate patients who underwent hypofractionated stereotactic body radiotherapy within the HypoFLAME trial (NCT02853110) were included in this study. A fractionation scheme of 5 × 7 Gy was used, with focal boosts up to 5 × 10 Gy to visible tumor nodule(s) on MRI. All patients had four implanted cylindrical gold FM (length: 5 mm, diameter: 1 mm) and were treated with online translation corrections based on the fiducial marker positions in kilovoltage (kV) images. Patients underwent MR imaging sessions after each weekly fraction at the University Medical Center of Utrecht between may 2016 and january 2017. During these repeated imaging sessions cine-MR images were acquired, resulting in a unique cine-MR imaging data set for every individual fraction. These cine-MR sessions consisted of 55 sequentially obtained 3D data sets ('dynamics'). Each cine-MR session consisted of a 3D balanced steady-state free precession (bSSFP) gradient echo sequence, acquiring one volume every 11 s over a time span of 10 min.

Tumor nodules visible on multiparametric MRI (T2 weighted, diffusion weighted imaging (DWI) and dynamic contrast enhanced (DCE)) were delineated as gross tumor volume (GTV). The whole prostate gland was considered as clinical target volume (CTV). The CTV included the GTV with an added margin of 4 mm, while excluding the OARs. The planning target volume (PTV) included the CTV with an added margin of 4 mm in all directions and was based on earlier experience with previously treated patients in our clinic. Seminal vesical contours were included based at the judgment of the treating physician. Rectum contours included the external

Table 1. Prostate planning constraints, where GTV is the gross tumor volume, CTV the clinical target volume (including the whole prostate gland) and PTV as the planning target volume.

VOI	Constraints		
GTV_50	V40Gy	>	99%
	V50Gy	<=	0.1 cc
CTV_35	V35Gy	>	99%
PTV_30	V30Gy	>	99%
PTV_33.25	V33.25Gy	>	99%
Rectum	Dmax	<	40 Gy
	V35Gy	<	2 cc
	V32Gy	<=	15%
	V28Gy	<=	20%
Bladder	V42Gy	<	1 cc
	V37Gy	<	5 cc
	V32Gy	<=	15%
	V28Gy	<=	20%
Urethra	Dmax	<	42 Gy
Femur heads	V28Gy	<=	5%

sphincter of the anus to the rectosigmoid flexure, where the anal canal was contoured from the external sphincter up to the internal sphincter (normally 3 cm). Additional OARs were the penile bulb, prostatic urethra and the bladder. Small bowel contour was only included when it was located near the PTV (den Hartogh *et al* 2019).

Treatment plans were generated in the Monaco treatment planning system (Elekta AB, Stockholm, Sweden) using dose to medium and patients were treated on conventional Agility Linacs with 5 mm multi-leaf collimator (MLC) leaf width and a total of 160 leaves. These treatment plans consisted of 10 MV volumetric arc therapy (VMAT) plans, using two full arcs and fulfilled the clinical constraints presented in table 1. The minimum segment width used was 0.5 cm with a maximum of 144 control points per arc. A grid spacing of 3 mm was used, with a statistical uncertainty per control point of 8%. Fiducial marker-based online corrections were applied during treatment.

For each cine-MR session a soft-tissue tracking algorithm was used to obtain the prostate intrafraction motion. This tracking method uses a delineation of the prostate body on the first cine-MR dynamic to rigidly register the prostate volume from subsequent cine-MR dynamics based on soft tissue contrast (de Muinck Keizer *et al* 2019a). The first cine-MR dynamic was then registered to the planning CT, based on the center of mass of the fiducial markers which were manually identified by a clinician (de Muinck Keizer *et al* 2019b). The fiducial marker based registration of the first cine-MR dynamic to the planning CT was used to transfer the local cine-MR motion to the CT coordinate system and maintained the rotation of the prostate, as the marker based registration was only performed using translations. This procedure mimics the daily re-positioning protocol we applied during actual treatment, in which only changes in translation based on the position of the fiducial markers are corrected for by a couch shift.

Then for each treatment fraction of the patient—assumed to have lasted 6 min for all patients on average—,the treatment delivery record was generated by proportionally splitting the plan into 11 s intervals based on the delivered Monitor Units. This led to 33 partial plans per fraction per patient for these dual arc VMAT plans. For each one of the 33 partial plans the dynamic volume—corresponding to the respective cine-MR rigid transformation—containing the necessary electron density values for the dose calculation was generated by rigidly transforming the planning CT. The body and bone structures from the CT were maintained and the rigidly transformed targets, bladder and rectum were assigned to water density (Kontaxis *et al* 2017a). The partial dynamic doses were calculated by using our in-house treatment planning system and research version of the GPUMCD dose engine (Hissoiny *et al* 2011). Then the respective inverse transformations were used to warp these partial dynamic doses back to the reference space.

For each fraction the motion-affected dose (INTRA_FR) was calculated by summing these 33 dynamic partial doses. Finally, for each patient the five fraction doses were added leading to the total treatment dose (INTRA). Both daily and total doses were compared to the original reference (REF) dose of the respective patient to assess the impact of the intrafraction motion.

3. Results

3.1. Motion analysis

A total of 143 cine-MR imaging sessions including 4719 dynamics among 29 patients were analyzed. The population intrafraction results during the simulated period of the VMAT treatment are provided in figure 1. Towards the end of this 6 min period, a group trend of 0.7 mm with a 95 percentile spread range of 6.9 mm in the anterior–posterior direction, −0.7 mm with a 95 percentile spread range of 6.3 mm in the cranial caudal direction and a rotation about the left–right axis of −0.4 degrees with a 95 percentile spread range of 9.9 degrees was observed.

3.2. Dosimetric analysis

Figure 2 shows a typical example of the dose distribution before and after dose accumulation. The dose accumulation as shown in this figure was performed for all fractions for one patient. The dose differences appear mainly in the bladder and rectum outside of the CTVs, depending on the prostate motion.

Figure 3 shows the D99% Dose Volume Histogram (DVH) point of the clinical target structures between REF and INTRA for all patients. The PTV_30 and PTV_33.25 had an average decrease of 3.1% ± 2.5% and 1.9% ± 1.7% respectively. For the clinically relevant target structures, the average D99% drop was 0.6% ± 1.0%, 0.2% ± 1.0% and 1.2% ± 2.0% for the CTV_30, CTV_35 and GTV_50 respectively. The mean dose of GTV_50 dropped by 1.0% ± 0.8%.

The PTVs ensured CTV_30 (seminal vesicles) coverage for all patients, CTV_35 (prostate body) coverage for 97% of the patients and GTV_50 (local boost) for 83% of the patients when strictly compared against the clinical constraints (table 1).

Figure 4 provides the boxplots for the V28Gy and V32Gy DVH points of the rectum and bladder. Both show very stable behavior between all patients compared to REF and are well within clinical constraints.

The Dmax DVH point of the rectum and urethra also remained stable and close to the REF plans, which can be observed in figure 5.

Depending on the underlying motion of the prostate, different types of motion-affected dose distributions can be observed. An overview of differences in intrafraction motion for a single patient with a high dosimetric impact and a single patient with a low dosimetric impact is provided in figure 6. The dosimetric impact in the DVH plots for these two patients is shown in figure 7. In this figure one case features low magnitude motion (figure 7(a)), while the second case has higher magnitudes of motion (figure 7(b)). In the first (lower magnitude) case the DVH lines for targets and OARs overlap between REF and INTRA doses, while in the second case (higher magnitude) both CTVs and the GTV have reduced coverage with the bladder entering the high dose region and receiving more dose while the rectum dose decreases.

Having the daily motion affected dose distributions (INTRA_FR) allows us to zoom into the individual fractions per patient. In the case of the patient corresponding to the total treatment dose in figure 7(b), on a fraction-by-fraction basis the CTV_30, CTV_35 and GTV_50 were underdosed by 1.9% ± 1.1%, 4.3% ± 2.5% and 5.6% ± 4.2% respectively (figure 8) while the bladder V32Gy point was violated in almost all fractions compared to REF (figure 9) .

4. Discussion

In this work we present a dose reconstruction study for twenty-nine previously treated prostate patients in our clinic with daily acquired post-treatment 3D cine-MR scans. We use a soft-tissue based rigid registration to extract translations and rotations of the prostate every 11 s and use these data as an intrafraction motion trace to perform accurate dose reconstruction.

The presented results demonstrate the potential dosimetric impact of intrafraction motion in SBRT prostate treatments with integrated GTV boost. Having considered the fact that the daily cine-MR data provide very realistic but not the true online motion that occurred during treatment, the 4 mm margins applied clinically in these SBRT treatments seem to overall ensure the safe delivery of the intended planned dose to the patients. For the sake of data completeness, a comparison is provided in the supplementary material (available at stacks.iop.org/PMB/65/025012/mmedia) with in-trafraction motion determined from the implanted fiducial markers (FM) and the cine-MR imaging sessions.

The PTVs present in these plans were adequate and maintained dose CTV coverage for all but one patient based on the planning constraints in table 1. A similar study using proton therapy showed comparable results in which intrafraction motion degrades the CTV coverage, but was maintained averaged over the course of the treatment (Tang *et al* 2013). More interesting is the GTV coverage which, given the smaller volume and steep boost dose gradient, was maintained for 25 out of 29 patients. The importance and clinical relevance of reduced accuracy in the boost dose delivery has to be further evaluated. The systematic caudal shift of the prostate

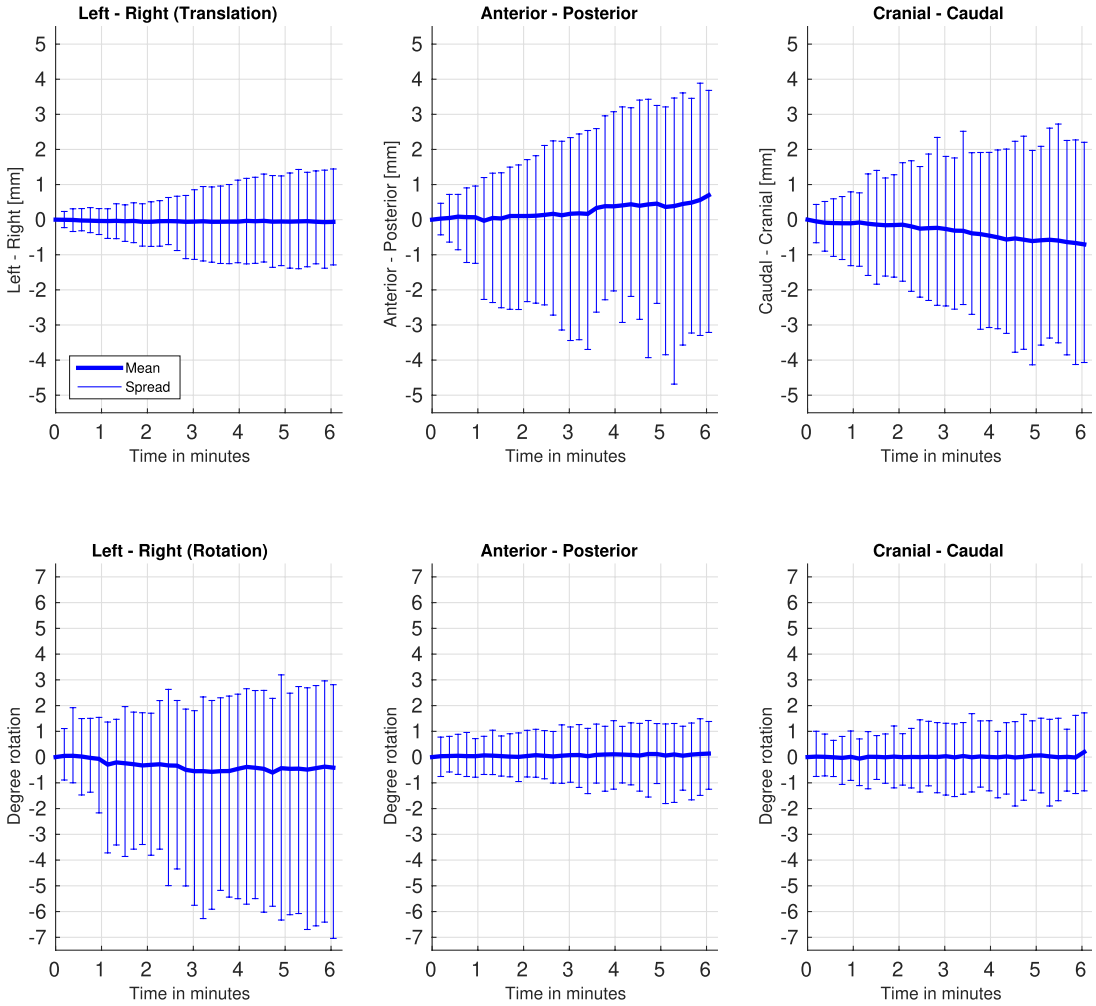

Figure 1. Overview of the population intrafraction motion for all 29 patients during the simulated period of the VMAT treatment. The graphs on the first row show the intrafraction translation, while the graphs on the second row show the intrafraction rotation. The increasing spread is visualized by the error bars, which show the 95 percentile intervals. An errorbar is shown for every 11 s, equal to the time period of one cine-MR dynamic.

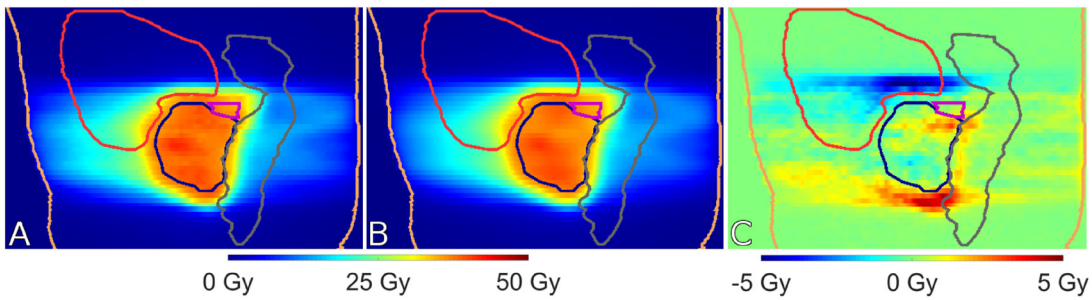

Figure 2. Sagittal slice from the planned dose (A), accumulated dose (B) and signed difference REF—INTRA (C) for one patient. CTV_35 (black, prostate body), CTV_30 (purple, seminal vesicles), bladder (red) and rectum (green) are shown.

of −0.7 mm due to bladder filling observed in the motion data was also overall observed in the motion-affected doses in which the bladder V32Gy was increased by 0.3% ± 1.9% and rectum V32Gy decreased by 0.6% ± 1.4% on average among the INTRA_FR daily accumulated dose distributions.

We have used 3D cine-MR with high spatial frequency to monitor the prostate motion instead of 2D surrogates (Litzenberg *et al* 2007, Li *et al* 2008). A limitation of this study is that we rely on rigid registration of the prostate and apply it to nearby OARs instead of deformable methods covering the whole patient anatomy. However besides rigid translations we also use the recorded prostate rotation for the anatomical motion tracking extracted from the 3D data which is known to be the principal motion component (de Boer *et al* 2005). The dynamic volumes used for dose calculation are generated by rigidly transforming the volumes of interest while maintaining

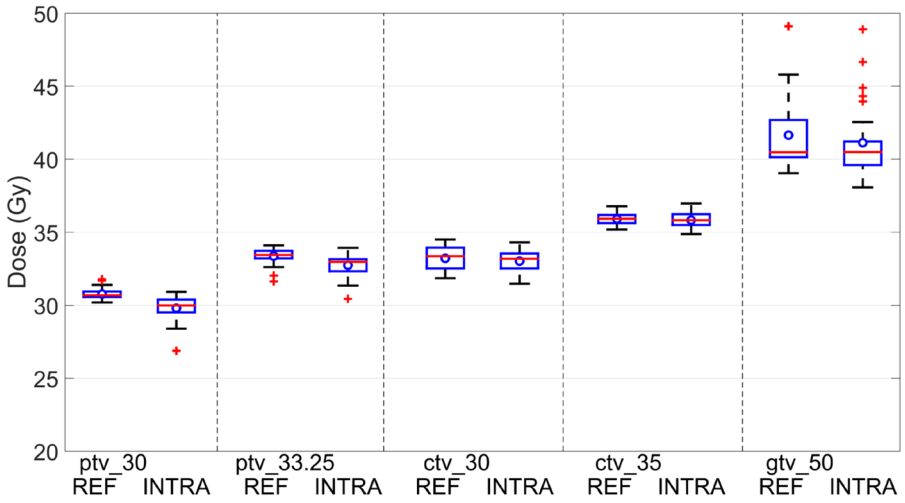

Figure 3. Boxplots including the D99% DVH point of the different target structures for all 29 patients. CTV_35 corresponds to the prostate body, CTV_30 to the seminal vesicles along with their corresponding PTV expansions and integrated boost GTV_50.

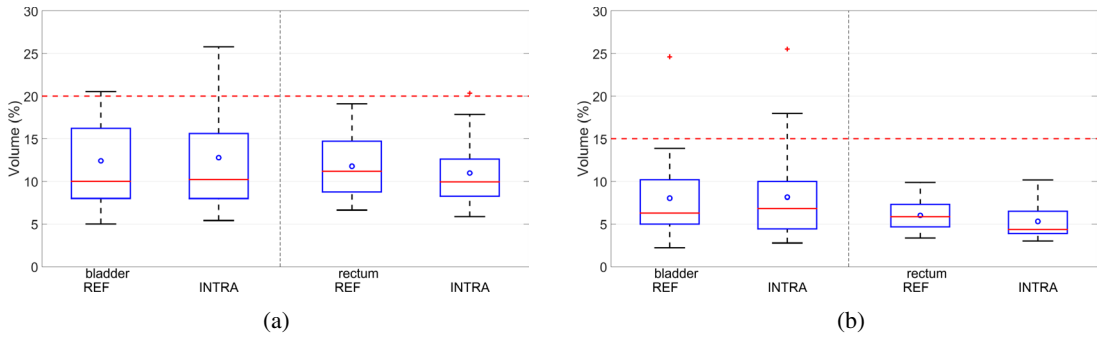

Figure 4. Bladder and rectum DVH boxplots for the accumulated treatment dose for all 29 patients. (a) Boxplots of the V28Gy patient average DVH point. (b) Boxplots of the V32Gy patient average DVH point.

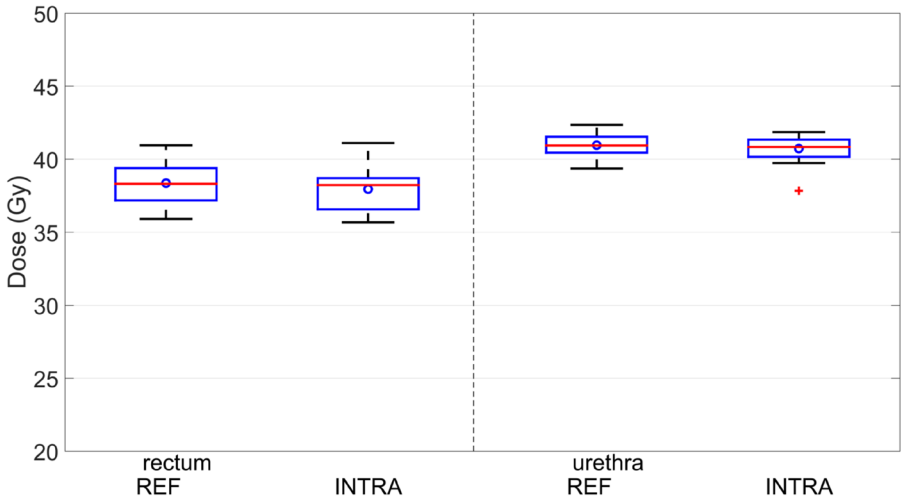

Figure 5. Boxplots of the Dmax DVH point of the rectum and urethra OARs for the accumulated treatment dose of all 29 patients.

the original body contour and bone structures. This method, compared to transforming the whole body of the patient, ensures that the calculated rigid prostate registration is not extrapolated to the whole anatomy and thus does not affect the dose calculation in an unrealistic way.

The next step is to use 3D deformable registration between the reference volume and the 3D cine-MR to yield 3D deformable vector fields (DVFs) and track the whole anatomy including the bladder, rectum and seminal vesicles. In the current work and all similar rigid-based methods, the reported dosimetric differences have an

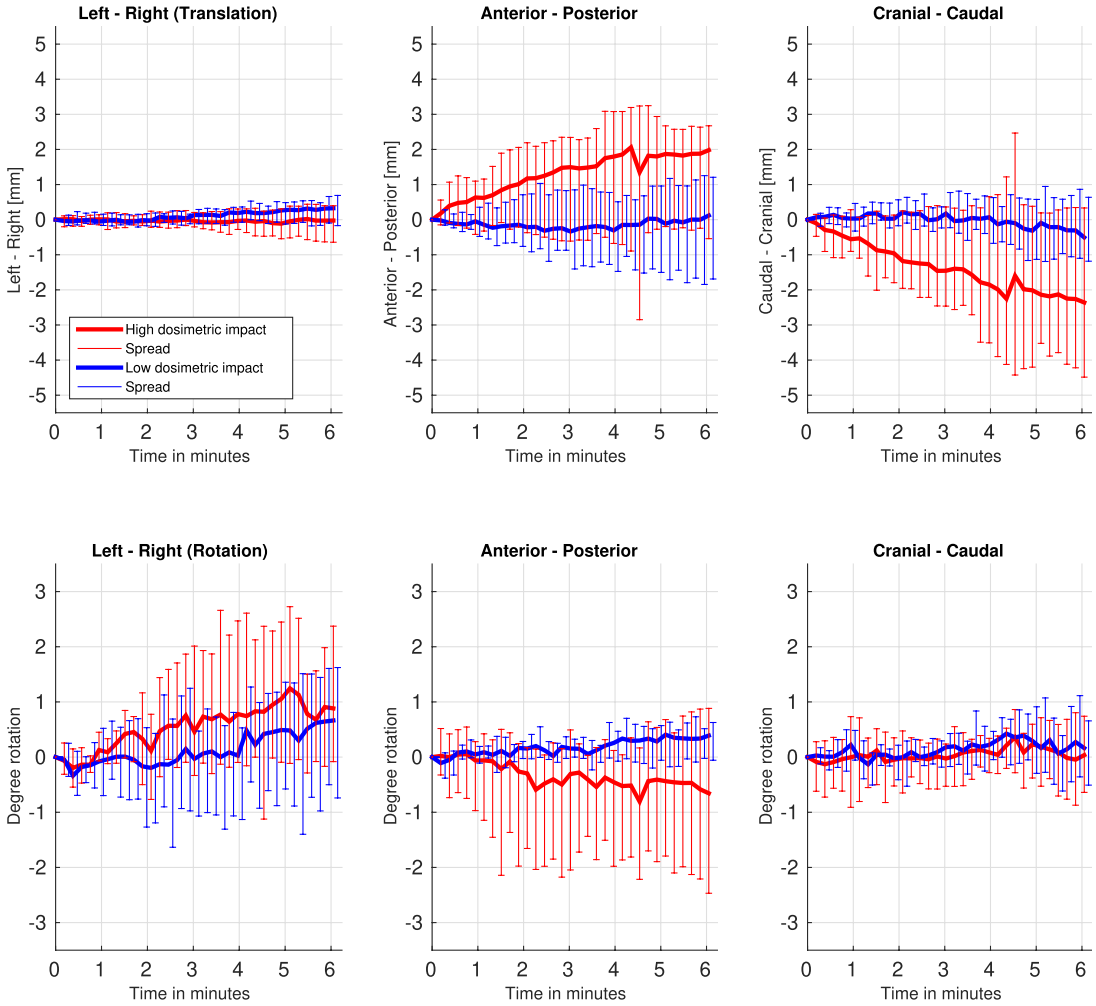

Figure 6. Overview of the intrafraction motion for two specific patients. One patient has a low dosimetric impact from intrafraction motion (blue). The other patient has a high dosimetric impact from intrafraction motion (red). The graphs on the first row show the intrafraction translation, while the graphs on the second row show the intrafraction rotation. The increasing spread is visualized by the error bars, which show the 95 percentile intervals. An errorbar is shown for every 11 s, equal to the time period of one cine-MR dynamic and includes five datapoints for the five imaging sessions of each patient.

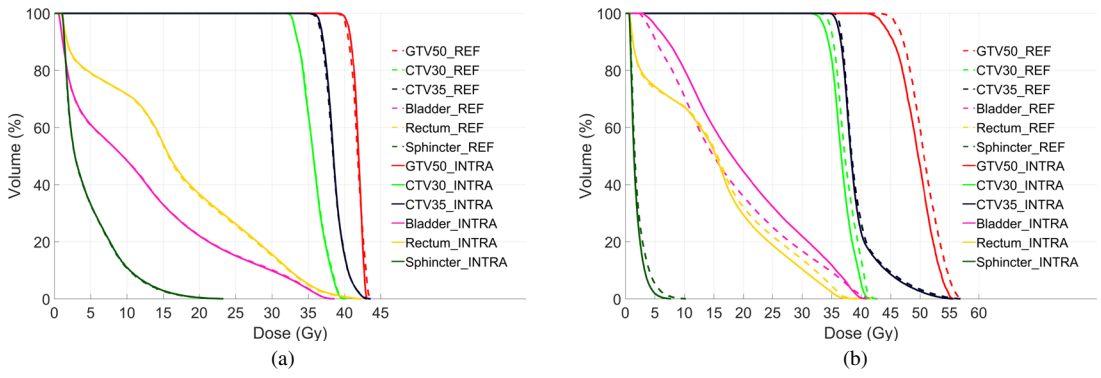

Figure 7. DVH plots showing the dosimetric impact due to intrafraction motion for two patients. Reference plans (REF) are plotted as dotted lines, while the motion affected results (INTRA) are plotted as continuous lines. CTV_30 contains the seminal vesicles, while CTV_35 contains the prostate body. (a) Low dosimetric impact. (b) High dosimetric impact.

increasing associated uncertainty as we go further away from the prostate. This means that the accumulated high dose levels of bladder and rectum (figures 4 and 5) are quite robust but parameters like the mean dose should be carefully read. In the same way, the dose variation of the CTV_30 including the seminal vesicles, which can be deformed in various ways compared to the prostate body, is non-trivial to interpret under the rigid assumption (figure 3).

While in this work the partial plans used for dose reconstruction are generated by splitting the patient VMAT plan into sub-plans, our dose reconstruction is also compatible with delivery records from linear accelerator

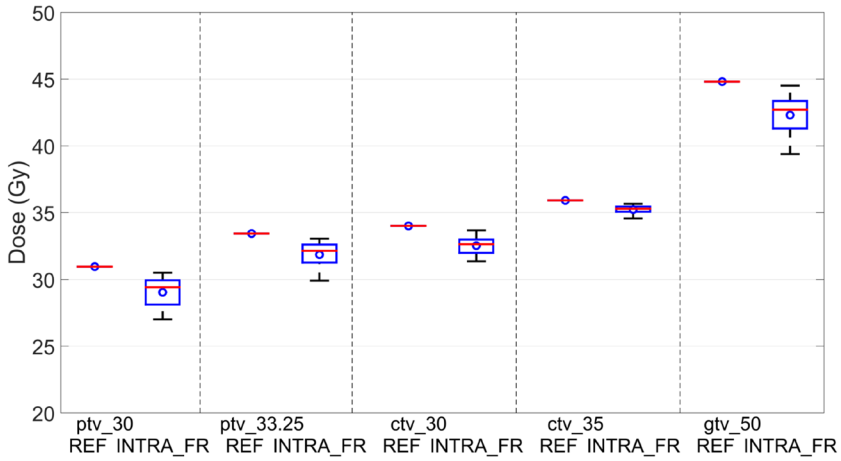

Figure 8. Boxplots of the target D99% DVH point for the fractions of a single patient with a high dosimetric impact due to intrafraction motion.

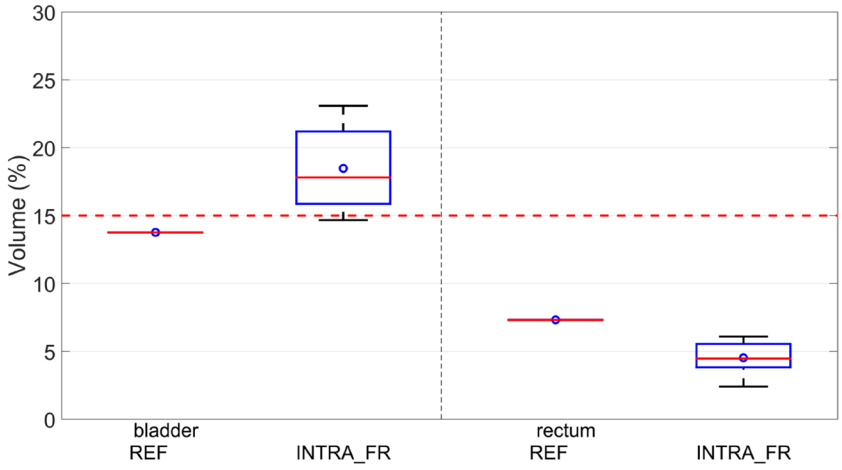

Figure 9. Boxplots of the V32Gy DVH point for the fractions of a single patient with a high dosimetric impact due to intrafraction motion.

log files that are generated during the actual radiation therapy for every fraction (Kontaxis *et al* 2017b). They contain all the relevant machine parameters timestamped on a high frequency rate and, thus when combined to high quality motion data, lead to accurate dose reconstruction. In this study, in the absence of such log files, we had to work with a fair assumption of the treatment times which was based on the observed average times during the treatment of several patients of this clinical protocol. The average delivery time of these 29 VMAT plans on a linac emulator was 5.5 min. Given the potential differences between the plans delivered on the emulator and actual linac (e.g. gantry movements, MLC, dose rate timings), we feel that the used 6 min is a fair assumption for the simulated treatments as described. In this respect, the dose reconstruction results and the conclusions in this study would not be significantly affected by slightly different treatment times and/or log file based calculations.

An extension of the current soft-tissue tracking would be the inclusion of the seminal vesicles as an additional region during the registration. As a first step prior to moving to full 3D DVFs, separate translation and rotation values for the seminal vesicles could be potentially used to get a more accurate dose estimation to the target volume.

We are presently developing a complete dose reconstruction pipeline, using the machine log files and online acquired cine-MR data during treatment for recently treated prostate patients on our MR-linac system. This will yield the first delivered dose reconstruction based on 4D anatomical data acquired during treatment. We expect that these dosimetric results will benefit from reduced uncertainty in comparison to this study, as then the cine-MR is acquired during the beam-on period and we will be able to make use of the machine log files. Despite the mentioned uncertainties, we do not expect significant changes for the dosimetric impact in the high-dose regions in future studies. Currently, we are focusing on optimizing the processing pipeline in terms of speed which becomes a key factor for such online applications, as all pipeline components including registration and dose calculation should be able to keep up with the imaging and radiation delivery.

This type of analyses will initially allow us to accurately track what we truly delivered daily to the patient and further enable to act upon if needed, by feeding the reconstructed dose into modular and fast planning pipelines to perform online plan adaptation (Kontaxis *et al* 2015). These online adaptive workflows along with the MR-linac soft-tissue imaging capabilities could enable extremely hypo-fractionated treatments with focal boosting and a safe margin reduction.

5. Conclusion

The dosimetric impact due to prostate intrafraction motion extracted by soft-tissue tracking on 3D cine-MR was simulated for previously treated patients in our clinic. The presented dose reconstruction pipeline and analysis are essential for establishing the actual delivered dose to the patient during the radiotherapy fractions. These results demonstrate that the clinically applied margins in these extremely hypofractionated prostate IGRT treatments are able to guarantee safe delivery of the planned dose to the patient. The emergence of MRI-guided radiotherapy further allows us to evaluate the impact of intrafraction motion with high spatial and temporal resolution. The next step is to apply such dose reconstruction pipelines on the actual MR-linac data. This will provide an invaluable decision making tool for preparing inter- and intra-fraction adaptation strategies for MR-guided radiotherapy that ensure continuous online target coverage and OAR sparing.

Acknowledgments

The authors would like to thank Elekta AB, Stockholm, Sweden for providing some of their research software tools.

References

Adamson J, Wu Q and Yan D 2011 Dosimetric effect of intrafraction motion and residual setup error for hypofractionated prostate intensity-modulated radiotherapy with online cone beam computed tomography image guidance *Int. J. Radiat. Oncol. Biol. Phys.* **80** 453–61

Alayed Y *et al* 2018 Dose escalation for prostate stereotactic ablative radiotherapy (SABR): late outcomes from two prospective clinical trials *Radiother. Oncol.* **127** 213–8

Azcona J D, Xing L, Chen X, Bush K and Li R 2014 Assessing the dosimetric impact of real-time prostate motion during volumetric modulated arc therapy *Int. J. Radiat. Oncol. Biol. Phys.* **88** 1167–74

Dasu A and Toma-Dasu I 2012 Prostate alpha/beta revisited–an analysis of clinical results from 14 168 patients *Acta Oncol.* **51** 963–74

de Boer H C, van Os M J, Jansen P P and Heijmen B J 2005 Application of the no action level (NAL) protocol to correct for prostate motion based on electronic portal imaging of implanted markers *Int. J. Radiat. Oncol. Biol. Phys.* **61** 969–83

De Leon J *et al* 2019 Reduced motion and improved rectal dosimetry through endorectal immobilization for prostate stereotactic body radiotherapy *Br. J. Radiol.* **92** 20190056

de Muinck Keizer D M, Kerkmeijer L G W, Maspero M, Andreychenko A, van der Voort van Zyp J R N, van den Berg C A T, Raaymakers B W, Lagendijk J J W and de Boer J C J 2019a Soft-tissue prostate intrafraction motion tracking in 3D cine-MR for MR-guided radiotherapy *Phys. Med. Biol.* **64** 235008

de Muinck Keizer D M, Pathmanathan A U, Andreychenko A, Kerkmeijer L G W, van der Voort van Zyp J R N, Tree A C, van den Berg C A T and de Boer J C J 2019b Fiducial marker based intra-fraction motion assessment on cine-MR for MR-linac treatment of prostate cancer *Phys. Med. Biol.* **64** 07NT02

den Hartogh M D *et al* 2019 Planning feasibility of extremely hypofractionated prostate radiotherapy on a 1.5 T magnetic resonance imaging guided linear accelerator *Phys. Imaging Radiat. Oncol.* **11** 16–20

Hissoiny S, Ozell B, Bouchard H and Després P 2011 GPUMCD: a new GPU-oriented Monte Carlo dose calculation platform *Med. Phys.* **38** 754–64

Huang C Y, Tehrani J N, Ng J A, Booth J and Keall P 2015 Six degrees-of-freedom prostate and lung tumor motion measurements using kilovoltage intrafraction monitoring *Int. J. Radiat. Oncol. Biol. Phys.* **91** 368–75

Keall P J *et al* 2014 The Australian magnetic resonance imaging–linac program *Semin. Radiat. Oncol.* **24** 203–6

Kontaxis C, Bol G H, Kerkmeijer L G W, Lagendijk J J W and Raaymakers B W 2017a Fast online replanning for interfraction rotation correction in prostate radiotherapy *Med. Phys.* **44** 5034–42

Kontaxis C, Bol G H, Stemkens B, Glitzner M, Prins F M, Kerkmeijer L G W, Lagendijk J J W and Raaymakers B W 2017b Towards fast online intrafraction replanning for free-breathing stereotactic body radiation therapy with the MR-linac *Phys. Med. Biol.* **62** 7233–48

Kontaxis C, Bol G, Lagendijk J and Raaymakers B 2015 A new methodology for inter-and intrafraction plan adaptation for the MR-linac *Phys. Med. Biol.* **60** 7485

Lagendijk J J W, Raaymakers B W and Van Vulpen M 2014 The magnetic resonance imaging–linac system *Semin. Radiat. Oncol.* **24** 207–9

Langen K M, Willoughby T R, Meeks S L, Santhanam A, Cunningham A, Levine L and Kupelian P A 2008 Observations on real-time prostate gland motion using electromagnetic tracking *Int. J. Radiat. Oncol. Biol. Phys.* **71** 1084–90

Li H S, Chetty I J, Enke C A, Foster R D, Willoughby T R, Kupellian P A and Solberg T D 2008 Dosimetric consequences of intrafraction prostate motion *Int. J. Radiat. Oncol. Biol. Phys.* **71** 801–12

Litzenberg D W, Hadley S W, Tyagi N, Balter J M, Ten Haken R K and Chetty I J 2007 Synchronized dynamic dose reconstruction *Med. Phys.* **34** 91–102

Loblaw A *et al* 2013 Prostate stereotactic ablative body radiotherapy using a standard linear accelerator: toxicity, biochemical, and pathological outcomes *Radiother. Oncol.* **107** 153–8

Mah D, Freedman G, Milestone B, Hanlon A, Palacio E, Richardson T, Movsas B, Mitra R, Horwitz E and Hanks G E 2002 Measurement of intrafractional prostate motion using magnetic resonance imaging *Int. J. Radiat. Oncol. Biol. Phys.* **54** 568–75

Morgan S C *et al* 2018 Hypofractionated radiation therapy for localized prostate Cancer: executive summary of an ASTRO, ASCO, and AUA evidence-based guideline *Pract. Radiat. Oncol.* **8** 354–60

Mutic S and Dempsey J F 2014 The ViewRay system: magnetic resonance–guided and controlled radiotherapy *Semin. Radiat. Oncol.* **24** 196–9

Pathmanathan A U *et al* 2018 Magnetic resonance imaging-guided adaptive radiation therapy: a game changer for prostate treatment? *Int. J. Radiat. Oncol. Biol. Phys.* **100** 361–73

Poulsen P R, Schmidt M L, Keall P, Worm E S, Fledelius W and Hoffmann L 2012 A method of dose reconstruction for moving targets compatible with dynamic treatments *Med. Phys.* **39** 6237–46

Tang S, Deville C, McDonough J, Tochner Z, Wang K K H, Vapiwala N and Both S 2013 Effect of intrafraction prostate motion on proton pencil beam scanning delivery: a quantitative assessment *Int. J. Radiat. Oncol. Biol. Phys.* **87** 375–82

Tree A, Jones C, Sohaib A, Khoo V and van As N 2013 Prostate stereotactic body radiotherapy with simultaneous integrated boost: which is the best planning method? *Radiat. Oncol.* **8** 228

van de Water S, Valli L, Aluwini S, Lanconelli N, Heijmen B and Hoogeman M 2014 Intrafraction prostate translations and rotations during hypofractionated robotic radiation surgery: dosimetric impact of correction strategies and margins *Int. J. Radiat. Oncol. Biol. Phys.* **88** 1154–60

van Herk M, McWilliam A, Dubec M, Faivre-Finn C and Choudhury A 2018 Magnetic Resonance Imaging–Guided radiation therapy: a short strengths, weaknesses, opportunities, and threats analysis *Int. J. Radiat. Oncol. Biol. Phys.* **101** 1057–60

Widmark A *et al* 2016 Extreme hypofractionation versus conventionally fractionated radiotherapy for intermediate risk prostate cancer: early toxicity results from the Scandinavian randomized phase III trial HYPO-RT-PC *Int. J. Radiat. Oncol. Biol. Phys.* **96** 938–9

Widmark A *et al* 2019 Ultra-hypofractionated versus conventionally fractionated radiotherapy for prostate cancer: 5-year outcomes of the HYPO-RT-PC randomised, non-inferiority, phase 3 trial *Lancet* **394** 385–95